CANCER

Disrupting the CD47-SIRPα anti-phagocytic axis by a humanized anti-CD47 antibody is an efficacious treatment for malignant pediatric brain tumors

Sharareh Gholamin,[1,2*†] Siddhartha S. Mitra,[1,2*‡] Abdullah H. Feroze,[1§] Jie Liu,[3‖] Suzana A. Kahn,[1,2] Michael Zhang,[1] Rogelio Esparza,[1] Chase Richard,[1¶] Vijay Ramaswamy,[4,5] Marc Remke,[4,5,6] Anne K. Volkmer,[2,7] Stephen Willingham,[2#] Anitha Ponnuswami,[8] Aaron McCarty,[2] Patricia Lovelace,[2] Theresa A. Storm,[2] Simone Schubert,[8] Gregor Hutter,[1**] Cyndhavi Narayanan,[3] Pauline Chu,[9] Eric H. Raabe,[10] Griffith Harsh IV,[11] Michael D. Taylor,[5] Michelle Monje,[1,2,8] Yoon-Jae Cho,[12] Ravi Majeti,[2,3] Jens P. Volkmer,[2‖] Paul G. Fisher,[8] Gerald Grant,[1] Gary K. Steinberg,[11] Hannes Vogel,[13] Michael Edwards,[1] Irving L. Weissman,[2,13††] Samuel H. Cheshier[1,2‡††]

Morbidity and mortality associated with pediatric malignant primary brain tumors remain high in the absence of effective therapies. Macrophage-mediated phagocytosis of tumor cells via blockade of the anti-phagocytic CD47-SIRPα interaction using anti-CD47 antibodies has shown promise in preclinical xenografts of various human malignancies. We demonstrate the effect of a humanized anti-CD47 antibody, Hu5F9-G4, on five aggressive and etiologically distinct pediatric brain tumors: group 3 medulloblastoma (primary and metastatic), atypical teratoid rhabdoid tumor, primitive neuroectodermal tumor, pediatric glioblastoma, and diffuse intrinsic pontine glioma. Hu5F9-G4 demonstrated therapeutic efficacy in vitro and in vivo in patient-derived orthotopic xenograft models. Intraventricular administration of Hu5F9-G4 further enhanced its activity against disseminated medulloblastoma leptomeningeal disease. Notably, Hu5F9-G4 showed minimal activity against normal human neural cells in vitro and in vivo, a phenomenon reiterated in an immunocompetent allograft glioma model. Thus, Hu5F9-G4 is a potentially safe and effective therapeutic agent for managing multiple pediatric central nervous system malignancies.

INTRODUCTION

Malignant pediatric brain tumors are etiologically distinct from adult brain tumors and responsible for the highest morbidity and mortality among all pediatric malignancies (*1*). Childhood malignant gliomas rapidly infiltrate adjacent brain tissue and are difficult to treat, with extremely poor prognosis (*2*, *3*). Pediatric embryonal tumors, namely, medulloblastoma (MB), atypical teratoid rhabdoid tumor (ATRT), and primitive neuroectodermal tumor (PNET), have moderately better survival after treatment; however, effective disease control is usually associated with severe physical and intellectual disabilities as well as later development of secondary malignancies (*3*–*5*). Moreover, when embryonal tumors occur in patients less than 3 years of age (as they often do), cranial-spinal irradiation therapy cannot be administered, making these tumors quite deadly in this age group, because they are not responsive to chemotherapies.

Tumor immune resistance and immune escape are hallmarks of primary malignant brain tumors (*6*). Recently, CD47 has been identified as a crucial protein expressed on the surface of cells in many cancers, allowing them to evade innate immune surveillance. CD47 overexpression is a common feature of hematologic and solid tumors (*7*–*10*). By binding and activating signal regulatory protein–α (SIRPα), an inhibitory protein expressed on the surface of myeloid cells, CD47 serves as an anti-phagocytic or "don't eat me" signal (*11*–*15*). Activation of SIRPα initiates a signaling cascade that inhibits the phagocytic activity of macrophages (*16*). The complex process of phagocytosis depends on the relative balance of pro-phagocytic ("eat me") and anti-phagocytic (don't eat me) signals. Most healthy normal cells, apart from aging red blood cells, lack expression of pro-phagocytic signals, but most cancer cells express pro-phagocytic signals on their cell surface. Although multiple eat me signals have been identified to date, only CD47 has been identified as the primary don't eat me signal (*13*, *17*–*20*). Therefore, by blocking CD47-SIRPα interaction, macrophages can be induced to selectively engulf cancer cells while sparing normal cells (*20*). Blocking the CD47-SIRPα interaction with a mouse anti-human CD47 monoclonal antibody (mAb) has the potential to

[1]Division of Pediatric Neurosurgery, Department of Neurosurgery, Lucile Packard Children's Hospital, Stanford University School of Medicine, Stanford, CA 94305, USA. [2]Institute for Stem Cell Biology and Regenerative Medicine and the Stanford Ludwig Cancer Center, Stanford University School of Medicine, Stanford, CA 94305, USA. [3]Division of Hematology, Department of Medicine, Stanford University School of Medicine, Stanford, CA 94305, USA. [4]Division of Haematology/Oncology, The Hospital for Sick Children, Toronto, Ontario M5G 1X8, Canada. [5]Division of Neurosurgery, Arthur and Sonia Labatt Brain Tumor Research Centre, The Hospital for Sick Children, Toronto, Ontario M5G 1X8, Canada. [6]Division of Pediatric Neurooncology, German Consortium for Translational Cancer Research, Heinrich-Heine-University Düsseldorf, 40225 Düsseldorf, Germany. [7]Department of Gynecology and Obstetrics, University of Düsseldorf, 40225 Düsseldorf, Germany. [8]Department of Neurology and Neurological Sciences, Stanford University School of Medicine, Stanford, CA 94305, USA. [9]Department of Comparative Medicine, Stanford University School of Medicine, Stanford, CA 94305, USA. [10]Division of Pediatric Oncology, Sidney Kimmel Comprehensive Cancer Center, Johns Hopkins University School of Medicine, Baltimore, MD 21287, USA. [11]Department of Neurosurgery, Stanford University School of Medicine, Stanford, CA 94305, USA. [12]Department of Pediatrics and Knight Cancer Institute, Oregon Health & Science University, Portland, OR 97231, USA. [13]Departments of Pathology and Developmental Biology, Stanford University School of Medicine, Stanford, CA 94305, USA.
*These authors contributed equally to this work.
†Present address: Division of Biology and Biological Engineering, California Institute of Technology, Pasadena, CA 91106, USA.
‡Corresponding author: Email: ssmitra@stanford.edu (S.S.M.); cheshier@stanford.edu (S.H.C.)
§Present address: Department of Neurological Surgery, University of Washington Medical Center, 325 9th Avenue, Campus Box 359924, Seattle, WA 98104, USA.
‖Present address: Forty Seven Inc., Menlo Park, CA 94025, USA.
¶Present address: Perelman School of Medicine, University of Pennsylvania, 3400 Civic Center Boulevard, Philadelphia, PA 19104, USA.
#Present address: Corvus Pharmaceuticals, Burlingame, CA 94010, USA.
**Present address: Department of Neurosurgery, University Hospital Basel, Spitalstrasse 21, CH-4031 Basel, Switzerland.
††These authors are co-senior authors.

effectively treat several solid tumors, including adult glioblastoma multiforme (GBM) (*11*–*15*, *21*), whereas normal (nonneoplastic) cells are not affected by CD47-blocking antibodies (*17*, *20*).

On the basis of this mechanism of action and its potent preclinical activity, we hypothesized that pediatric brain tumors would be susceptible to blocking CD47 antibodies. A humanized anti-CD47 antibody with a human immunoglobulin G4 (IgG4) scaffold (Hu5F9-G4) was engineered to minimize the recruitment of antibody Fc-dependent effector functions and to reduce immunogenicity of the antibody (*22*). We tested the antitumor activity of Hu5F9-G4 in human patient-derived primary xenograft models from five of the most malignant pediatric brain tumors: group 3 MB, ATRT, PNET, epidermal growth factor receptor–amplified pediatric GBM (pGBM), and diffuse intrinsic pontine glioma (DIPG) harboring histone 3.3 K27M mutation.

Here, we report that Hu5F9-G4 demonstrates potent activity against these primary malignant pediatric brain tumor types, regardless of histologic classification or molecular origin. Furthermore, Hu5F9-G4 was highly efficacious against primary tumor and subarachnoid dissemination, with negligible activity against normal neural cells.

RESULTS

Hu5F9-G4 induces phagocytosis and inhibits growth of human group 3 MB

MB has been molecularly classified into four core subgroups: WNT, SHH, group 3, and group 4. The 5-year overall survival of group 3, the most aggressive subgroup, is 50%, and about 30% in patients presenting with metastases at the time of diagnosis (*4*). Ubiquitous expression of CD47 was observed in the Boston, Heidelberg, and Toronto MB gene expression data sets (fig. S1, A to D) (*4*, *23*). Gene expression analysis suggests higher CD47 expression in metastatic regions of MB as compared to the primary site tumor (fig. S1E). Analysis of CD47 surface expression by flow cytometry on human group 3 MB tissue specimens showed 86 to 99.4% of cells expressing CD47 on their surface (fig. S1F). MB lines also showed cell surface exposure of calreticulin (CRT), a pro-phagocytic eat me signal, by flow cytometry (fig. S1G). We therefore hypothesized that blocking the CD47-SIRPα interaction by Hu5F9-G4 will facilitate phagocytosis of group 3 MB tumors by macrophages, resulting in elimination of the primary tumor as well as metastases.

In vitro phagocytosis assays with human peripheral blood mononuclear cell (PBMC)–derived macrophages established the ability of Hu5F9-G4 to induce phagocytosis of primary and xenograft-derived MB cells (figs. S2, A to D, and S3, A and B). The engulfment of tumor cells by macrophages was verified by cell sorting of $CD11b^+CD14^+calcein^+$ cells and subsequent Wright-Giemsa staining after cytospin (fig. S4, A to C). The administration of Hu5F9-G4 in mice bearing MB promoted extensive in vivo phagocytosis of group 3 MB cells (fig. S4, D to F).

We tested the in vivo antitumor effect in an orthotopic xenograft model in immunodeficient NSG mice that lack B, T, and natural killer (NK) cells but retain macrophages with phagocytic potential (*13*). Two primary group 3 (SU_MB002 and SU_MB009) and three commercial *cMYC*-amplified MB cell lines (D283, D425, and D425s), expressing green fluorescent protein (GFP) and luciferase, were transplanted into the cerebellum of NSG mice. Tumor engraftment was verified by bioluminescence imaging (BLI) of all transplanted mice and by hematoxylin and eosin (H&E) staining of a representative mouse from each group. MB was seen at the primary site (cerebellum) and disseminated to the leptomeninges (fig. S5, A to G). Intraperitoneal treatment with Hu5F9-G4 was initiated after randomization by BLI flux values to ensure that tumors were of equal size in the treatment and control groups (Fig. 1A). BLI showed a significant reduction in tumor burden after treatment with Hu5F9-G4 (SU_MB002; $P = 0.0057$) (Fig. 1, B and C). Kaplan-Meier analysis of mice injected with SU_MB002 showed significant improvement in survival of the Hu5F9-G4–treated cohort compared with the control ($P < 0.0001$) (Fig. 1D).

Tumor burden in treated versus control mice was verified using H&E staining. H&E staining of brains from Hu5F9-G4–treated mice showed no tumor cells or minimal residual tumor in the cerebellum or leptomeninges, whereas control mouse brains harbored large tumors in the cerebellum with extensive leptomeningeal spread (Fig. 1E). To assess tumor cell engulfment by macrophages in vivo, we performed immunohistochemical (IHC) staining on orthotopic xenografted brains treated with either control or Hu5F9-G4. Substantial macrophage recruitment was detected in the group treated with Hu5F9-G4, concentrated around sites of residual tumor upon staining for F4/80, a pan-macrophage marker. However, control animals with substantial tumor burden showed limited but diffuse presence of macrophages (Fig. 1F).

To test the effect of Hu5F9-G4 on multiple primary patient-derived MB lines, we conducted a similar set of experiments using D283, D425, and D425s lines (fig. S6, A to Q). The tumor cells were transplanted into the cerebellum of NSG mice. Tumor engraftment was verified by BLI, and treatment scheme was determined after randomization (fig. S6, A, G, and M). Significant reduction in BLI ($P < 0.0001$) was seen in mice xenografted with D425 and D283 followed by Hu5F9-G4 treatment (fig. S6, B, C, H, and I). Mice implanted with D425, D283, and D425s and treated with Hu5F9-G4 showed significant extension in survival ($P < 0.0001$, $P < 0.0001$, and $P = 0.0018$; fig. S6, D, J, and P).

IHC and staining against F4/80 protein were performed on dissected brains after the treatment. A reduced tumor burden and substantial macrophage recruitment were detected in the groups treated with Hu5F9-G4, whereas the control brains showed large tumors with negligible presence of macrophages (fig. S6, E, F, K, L, N, and O, and table S1).

We tested for dose-dependent effect of the mAb in vivo and found that the survival of animals with D425s xenografts was significantly improved by increasing the dose of Hu5F9-G4 from 250 to 450 μg per mouse, three times per week ($P = 0.0023$) (fig. S6Q). Qualitative evaluation of behavior revealed that mice treated with Hu5F9-G4 displayed normal feeding and movement, whereas those treated with the control were cachectic, hunched, and lethargic (movies S1 and S2).

Because metastatic recurrence of MB with *MYC* amplification has near 100% fatality in children (*1*, *4*), we tested the effect of Hu5F9-G4 on spinal metastases from *MYC*-amplified group 3 cell lines. Hu5F9-G4 treatment was able to clear metastases from the spine in this xenograft model (Fig. 1, G to I), thus establishing the efficacy of Hu5F9-G4 treatment in all regions of the central nervous system (CNS). Similar results were seen in D425 xenografted mice, where no spinal metastasis was observed in Hu5F9-G4–treated mice compared with 80% of the mice in the control cohort (fig. S6B). Furthermore, a therapeutic dose of Hu5F9-G4 administered intraperitoneally was around 200 μg/ml in blood serum and 20 μg/ml in cerebrospinal fluid (CSF), proving penetration of the blood-brain barrier by Hu5F9-G4 (fig. S7, A to C). In addition, we detected the presence of Hu5F9-G4 in CSF of non–tumor-bearing mice, establishing its ability to traverse the blood-brain barrier even when no tumor is present (fig. S7B). IHC staining for IgG4 in the brains of tumor-bearing mice treated with Hu5F9-G4 revealed high staining of IgG4 in

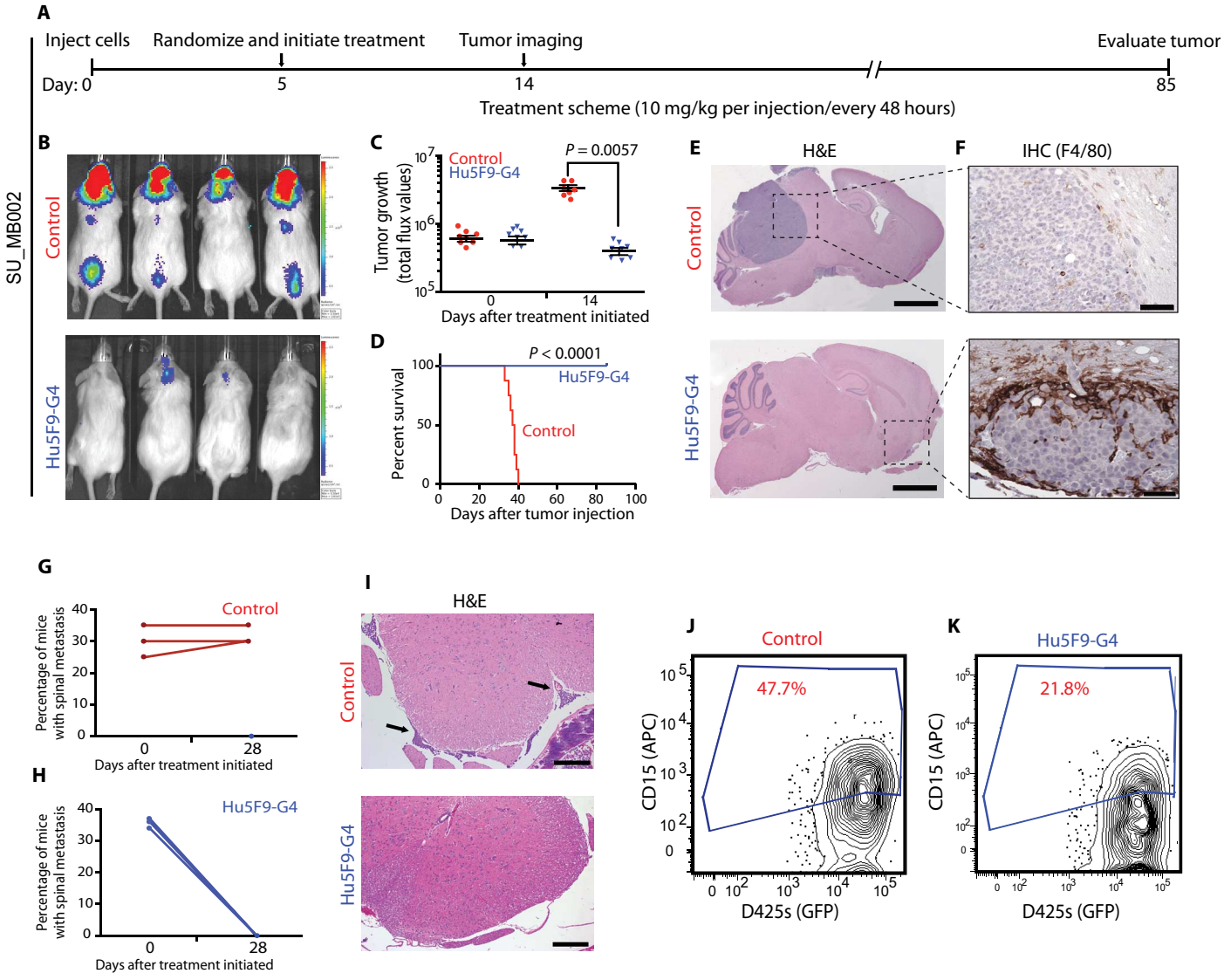

Fig. 1. Hu5F9-G4 inhibits primary and metastatic MB in vivo. (**A**) Treatment scheme for the evaluation of in vivo efficacy of Hu5F9-G4. (**B** and **C**) Representative image (B) and quantitation of BLI (C) of patient-derived *cMYC*-amplified MB (shown as SU_MB002) xenograft from Hu5F9-G4–treated and control mice. Hu5F9-G4–treated mice showed significant decrease in tumor burden compared with control mice ($P = 0.0057$). (**D**) Hu5F9-G4 significantly increased survival of mice with *cMYC*-amplified tumors ($n = 8$ per group; $P < 0.0001$, log-rank analysis). (**E**) H&E staining of sagittal sections from mice treated with Hu5F9-G4 showed reduction of tumor size at the primary cerebellar site of transplantation as well as elimination of the leptomeningeal disease (scale bars, 2 mm). (**F**) Immunostaining with anti-F4/80 antibody showed increased macrophage accumulation at tumor sites after treatment with Hu5F9-G4 (scale bars, 50 μm). (**G** and **H**) Percentage of mice with spinal metastasis before and after treatment with either control (G) or Hu5F9-G4 (H). Each line represents an independent experiment ($n = 3$) with 8 to 10 mice in each arm per experiment. (**I**) H&E staining of spinal cord sections from mice treated with control or Hu5F9-G4 (scale bars, 200 μm). Metastatic tumors are shown by arrows. (**J** and **K**) Representative flow cytometric plots of dissociated NSG mouse brains transplanted with human MB cells. Human MB-initiating cells were identified as $CD15^+GFP^+msLIN^-$ cells. Treatment with Hu5F9-G4 (J) reduced the percentage of human MB-initiating cells compared to the control counterpart (K). APC, allophycocyanin.

the treated group and no sign of staining in the control, further confirming the penetration of Hu5F9-G4 to brain tumor tissue in treated mice (fig. S7D).

To quantitate the recruitment of macrophages within the tumor area, we sacrificed Hu5F9-G4–treated mice and controls after five injections of Hu5F9-G4 (one injection every other day), extracted the brains, and identified the tumors by GFP under a fluorescence stereomicroscope. Engrafted tumors were microdissected, dissociated to single cells, and analyzed for the presence of macrophages by the expression of CD11b and F4/80 (fig. S8, A to F). Flow cytometric analysis showed significantly higher frequency of intratumoral macrophages ($P = 0.0143$) in the treated (15.7%) versus the control (3.32%) groups (fig. S8, C, E, and F). Together, these results demonstrate that Hu5F9-G4 treatment crosses the blood-brain barrier and has potent antitumor activity against group 3 MB in vivo. All mice bearing MB cell lines (SU_MB002, D425, D283, D425s, and SU_MB009; fig. S9, A to E) responded to Hu5F9-G4 treatment with extended survival, less tumor burden, and more macrophages present in the residual tumor versus controls.

Because the growth of MBs depends on $CD15^+$ cancer stem cells (CSCs) (*24*, *25*), we tested the ability of Hu5F9-G4 to target $CD15^+$

MB CSCs. Flow cytometric analysis of MB xenografts 2 days after the sixth injection of Hu5F9-G4 treatment showed a lower frequency of human $CD15^+$ cells in the Hu5F9-G4–treated mice than in the controls ($P = 0.02$) (Fig. 1, J and K, and fig. S3B). Thus, $CD15^+$ group 3 MB CSCs are also targeted by Hu5F9-G4 treatment.

Continuous intraventricular infusion of Hu5F9-G4 inhibits leptomeningeal metastasis of MB

Recurrence of MB is frequently associated with metastasis, and a substantial percentage of group 3 patients harbors metastatic disease at presentation (*26*). Given that MB metastasis typically occurs along the CSF pathways within the leptomeningeal spaces, we wanted to explore the possibility of enhanced targeting of metastatic sites via direct delivery of antibody into the CSF. Mice with cerebellar D425 xenografts presenting with forebrain and spinal metastasis were randomized on the basis of BLI flux values, divided into control and treated groups, and implanted with osmotic pumps delivering Hu5F9-G4 (150 μg/day) to the lateral ventricle via direct cannulation (Fig. 2A). This Hu5F9-G4 dose is comparable to the quantity of antibody received via systemic treatment over the same period. Hu5F9-G4 is stable at ambient temperature for at least 56 days (fig. S10A). Tumor burden was evaluated by BLI after 14 days of treatment (Fig. 2, B and C). Intraventricular delivery of Hu5F9-G4 was associated with a significantly longer survival ($P = 0.0027$) (Fig. 2D); however, this survival advantage was shorter than that associated with systemic treatment (fig. S6D). Histological analysis of mice with intraventricular treatment showed that, despite elimination of leptomeningeal metastases with increased recruitment of macrophages, the tumor at the primary site was not significantly affected (Fig. 2E). However, intraventricular delivery of Hu5F9-G4 did provide an accelerated antitumor effect on spinal and forebrain leptomeningeal metastases as seen by both histology (Fig. 2, E and F) and BLI (Fig. 2, G and H) when compared with systemic treatment. Mice were weighed before and after treatment, and no weight loss was observed in mice treated with intraventricular delivery of Hu5F9-G4 compared with the control (Fig. 2I). These results revealed increased potency of Hu5F9-G4 against leptomeningeal disease with intraventricular administration to the CSF, but little to no effect on the primary tumor at the cerebellum, indicating that these two locations have separate barriers to Hu5F9-G4 penetration.

Hu5F9-G4 eliminates MB cells but not normal human CNS cells in a treatment model

Current regimens of radiation and chemotherapy cause considerable and often permanent side effects because of their toxicity to normal cells, particularly to a child's developing brain (*27*). Thus, we assessed whether Hu5F9-G4 results in any toxicity to human-derived neural cells. No loss in viability or proliferation was observed in normal human neural progenitor cells (NPCs) after 5 days of treatment with Hu5F9-G4 at a concentration as high as 1 mg/ml (fig. S11A). Furthermore, Hu5F9-G4 failed to induce phagocytosis of normal human NPCs or their differentiated progeny, namely, neurons and astrocytes (fig. S11B).

To further examine whether Hu5F9-G4 could differentiate between tumor and normal cells while selectively targeting cancer cells, we coincubated tumor cells and normal human NPCs and exposed the combination to Hu5F9-G4 in the presence of human PBMC-derived macrophages (Fig. 3A). Flow cytometric analysis revealed sevenfold higher phagocytosis of tumor cells compared with phagocytosis of NPCs (Fig. 3, B and C). The phagocytosis of NPCs was not above background levels even in the presence of active phagocytosis of tumor cells in vitro.

To determine whether Hu5F9-G4 has an in vivo bystander effect on normal human NPCs, we developed a surrogate assay. Previously, we had demonstrated the ability of human fetal brain-derived NPCs to engraft into NSG mouse brains and to migrate and differentiate in a site-appropriate fashion into neurons, astrocytes, and oligodendrocytes (*28*, *29*). Using this model, we injected nontransduced human MB cells (SU_MB002) into mice that had previously been engrafted with luciferase-expressing human neural precursor cells. These mice, harboring both human tumor and normal human CNS cells, were then treated with Hu5F9-G4 or the control (Fig. 3D). In this case, BLI signal was observed and measured from the engrafted normal human NPCs and their progeny cells and not from the tumor cells. No significant change was observed in BLI signal after treatment with Hu5F9-G4, suggesting robust and continued cellular proliferation and viability even in the presence of Hu5F9-G4 treatment (Fig. 3, E and F). The antitumor activity of Hu5F9-G4 was confirmed by Kaplan-Meier survival analysis (Fig. 3G). Therefore, little, if any, elimination of normal human CNS cells was observed in the setting of potent in vivo antitumor activity of Hu5F9-G4 against MB cells.

Hu5F9-G4 induces phagocytosis and inhibits growth of human pediatric ATRT and PNET xenografts

ATRT and PNET are highly malignant pediatric brain tumors with poor prognosis. We hypothesized that CD47 is expressed on the surface of ATRT and PNET cells and that Hu5F9-G4 treatment would enable the phagocytosis of these tumor cells. Expression analysis of the limited data set available ($n = 18$) showed CD47 expression in all ATRT tumors (fig. S12, A and B). Flow cytometric analysis of ATRT and PNET primary cell lines derived from patient surgical samples showed surface expression of CD47 and CRT on almost all cells (Fig. 4, A and B, and fig. S12, C and D). The normal neural stem cell lines expressed a negligible amount of CRT on the cell surface, suggesting the specificity of this marker as a pro-phagocytic eat me signal on cancer cells (fig. S12D). Similarly, fresh-frozen surgical samples exhibited widespread expression of CD47 in both tumor types by immunofluorescence staining (Fig. 4, C and D). In vitro phagocytosis of both tumor types was about fivefold higher upon treatment with Hu5F9-G4 versus controls (Fig. 4E and fig. S13A). We intracranially transplanted GFP- and luciferase-expressing SU_ATRT002 or sPNET cells into NSG mouse brains and started treatment after tumor engraftment was verified by BLI. Subsequent intraperitoneal treatment (Fig. 4F) of SU_ATRT002 xenografts with Hu5F9-G4 resulted in a significant reduction in tumor growth and possible elimination of the tumor in some mice compared with the controls as observed by BLI ($P < 0.0001$) (Fig. 4, G and H). Kaplan-Meier analysis demonstrated increased overall survival of mice treated with Hu5F9-G4 compared with controls ($P < 0.0001$) (Fig. 4I). H&E staining of brains xenografted with ATRT showed reduced tumor burden in the treated group compared with controls (Fig. 4J). IHC staining with the macrophage marker F4/80 indicated increased infiltration of macrophages at the tumor site in treated cohorts versus control (Fig. 4K). These results indicate that Hu5F9-G4 has extensive in vitro and in vivo activity against ATRT.

Similarly, to test the efficacy of Hu5F9-G4 against PNETs, we randomized intracranial xenografts of luciferase-expressing sPNET cells based on BLI into treatment and control groups (Fig. 4L). BLI flux analysis after 28 days of treatment revealed a significant decline in tumor

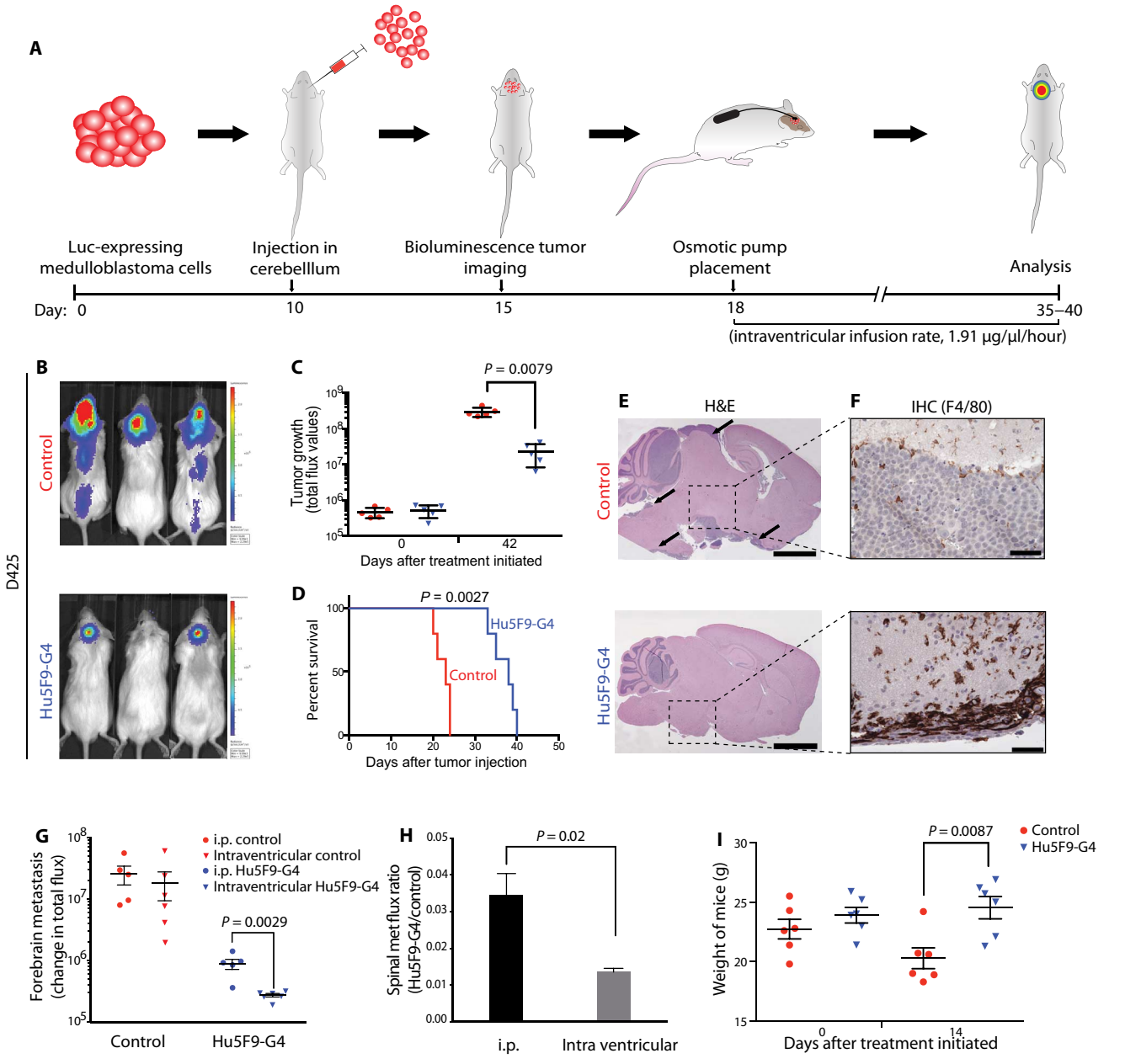

Fig. 2. Intraventricular infusion of Hu5F9-G4 accelerates antimetastatic activity. (**A**) Schematic representation of intraventricular infusion experiment. Osmotic pumps loaded with Hu5F9-G4 were implanted into mice for direct ventricular infusion into the lateral ventricle after tumor formation was confirmed by BLI. (**B** and **C**) Representative BLI images (B) and quantitation (C) after 30 days of intraventricular infusion. (**D**) Kaplan-Meier analysis of mice infused with Hu5F9-G4 and control ($n = 10$ per group; $P = 0.0027$, log-rank analysis). (**E**) H&E staining reveals the presence of primary cerebellar tumor in both the control and Hu5F9-G4–treated mice, with lack of ventricular and leptomeningeal metastasis in the forebrain (scale bars, 2 mm) of Hu5F9-G4–treated mice. (**F**) Infiltration of macrophages in Hu5F9-G4–treated mice as visualized by F4/80 macrophage staining (scale bars, 50 µm). (**G**) Comparative analysis of tumor burden in mice treated by intraperitoneal (i.p.) injection (circle) or intraventricular infusion (triangle), showing accelerated antitumor effect on forebrain leptomeningeal tumor spread with intraventricular infusion. (**H**) Ratio of spinal metastasis flux in Hu5F9-G4–treated to control mice after 14 days of treatment. (**I**) Weight of mice with intraventricular Hu5F9-G4 or control 14 days after initiation of treatment.

burden of mice treated with Hu5F9-G4 ($P = 0.0079$) (Fig. 4, M and N). Subsequent survival analysis showed the extended survival in a treated group with Hu5F9-G4 ($P < 0.001$) (Fig. 4O). H&E staining of brains xenografted with sPNET revealed minimal tumor burden in mice treated with Hu5F9-G4 (Fig. 4P). IHC staining against F4/80 protein showed the increased entrance of macrophages into the tumor site in Hu5F9-G4–treated mice (Fig. 4Q).

Hu5F9-G4 induces phagocytosis and inhibits tumor growth of human pGBM and DIPG

Pediatric high-grade gliomas are deadly tumors and include pGBM and DIPG. pGBM has a median survival of 5 years (*2*), with few patients responding to current treatments. Children with DIPG usually succumb to disease in less than 1 year from diagnosis (*30*). We hypothesized that CD47 is highly expressed on pGBM and DIPG, and

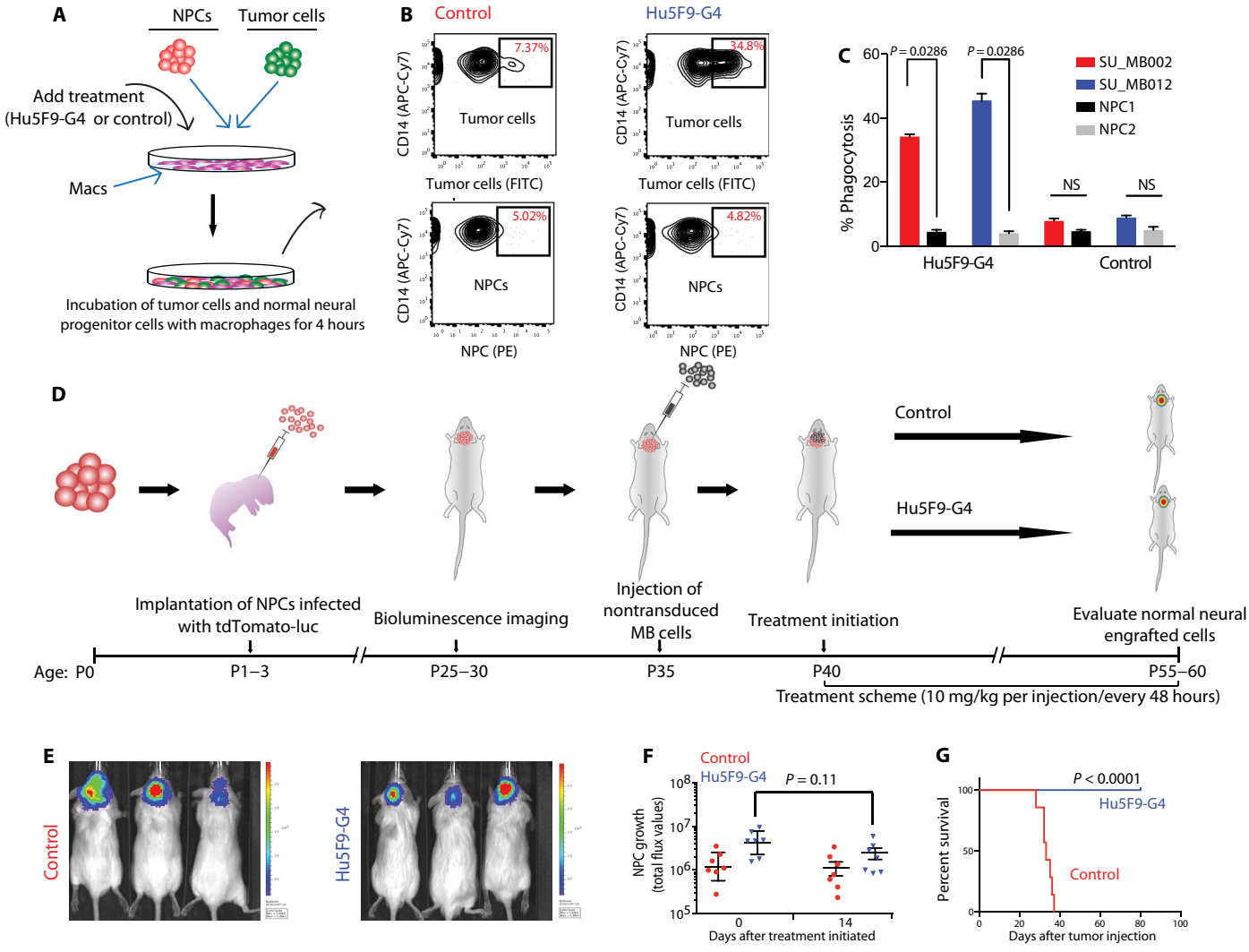

Fig. 3. Hu5F9-G4 selectively targets tumor cells in vitro and in vivo. (**A**) In vitro experimental design to assay Hu5F9-G4 selectivity. Color-coded NPCs (red) and SU_MB002 tumor cells (green) were coincubated with macrophages (macs) in the presence of Hu5F9-G4 and assayed for phagocytosis. (**B** and **C**) Flow cytometric (B) and histogram (C) plots show more phagocytosis of tumor cells by macrophages in the presence of Hu5F9-G4, whereas the percentage of phagocytized NPCs was low with both control and Hu5F9-G4 treatments. The color-coded tumor cells and NPCs were analyzed in the fluorescein isothiocyanate (FITC) and phycoerythrin (PE) channels, respectively. NS, not significant. (**D**) Schematic representation of experimental design to test for in vivo cytotoxic effect on human NPCs in tumor-bearing mice. Unlabeled human MB cells (SU_MB002) were injected into mice with previously engrafted luciferase-expressing human NPCs and treated with Hu5F9-G4 or control. Note that in this experiment, BLI was observed from the human NPCs and not from the tumor cells. (**E** and **F**) BLI images (E) and measures (F) show no statistically significant change in growth of NPCs in mice treated with control or Hu5F9-G4 [$n = 8$ (control) and $n = 7$ (Hu5F9-G4); $P = 0.11$]. (**G**) Improved survival was seen in mice treated with Hu5F9-G4 compared to the control group ($P < 0.0001$).

that using Hu5F9-G4 to block CD47 on the cell surface of pGBM or DIPG would enable the phagocytosis of pHGG cells, resulting in an inhibition or elimination of the tumor. To evaluate the expression of CD47 in pHGG, we interrogated multiple published gene expression data sets for CD47 expression. All data sets indicated ubiquitous expression of CD47 in pGBM and DIPG (fig. S12, A and B) (*4*, *31*–*37*). Pediatric glioma-initiating cell (PGIC) lines derived from either post-mortem DIPG rapid autopsy samples (SU_DIPGVI, SU_DIPGXIII, and JHH_DIPGI) or patient surgical pGBM samples (SU_pGBM001 and SU_pGBM002) showed high expression of CD47 by flow cytometric analysis (Fig. 5, A and B, and fig. S12C). Furthermore, flow cytometric analysis showed surface expression of CRT on pGBM and DIPG cells (fig. S12D). Immunofluorescence staining of fresh-frozen patient samples showed expression of CD47 in primary tumors (Fig. 5, C and D). Using flow cytometry (gating strategy shown in fig. S3A), we evaluated the ability of Hu5F9-G4 to induce the phagocytosis of dissociated primary PGICs in vitro. In contrast to PGICs treated with human IgG, PGICs treated with Hu5F9-G4 were efficiently phagocytosed by macrophages derived from PBMCs (Fig. 5, E to H, and fig. S13, B to D). We further observed coexpression of the neural/tumor progenitor markers, Olig2 and Nestin, with CD47 (fig. S14, A and B) (*38*–*40*). We intracranially transplanted GFP- and luciferase-expressing SU_pGBM002 cells into NSG mouse brains and started treatment after tumor engraftment was verified by BLI (Fig. 5I). Intraperitoneal treatment with Hu5F9-G4 resulted in a significant reduction in tumor growth, with elimination of the tumor in SU_pGBM002 ($P = 0.0003$) (Fig. 5, J and K). Mice treated with Hu5F9-G4 showed significant survival benefit compared to control

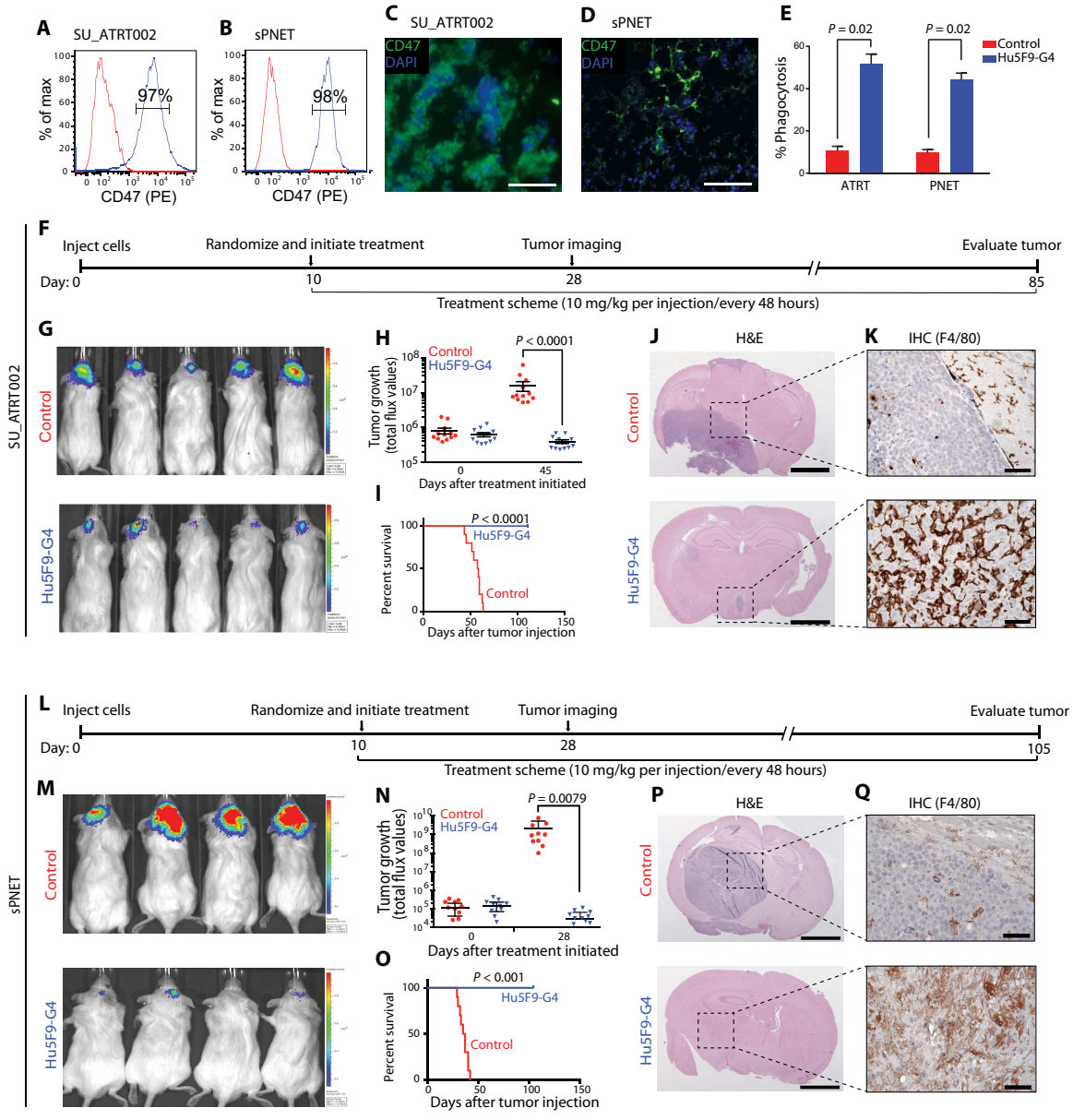

Fig. 4. Hu5F9-G4 targets human ATRT and PNET in vitro and in vivo. (**A** and **B**) Flow cytometric plots of cell surface expression of CD47 on primary ATRT (A) and sPNET (B) cell lines. More than 95% of cells express CD47 on their surface. (**C** and **D**) Expression of CD47 on fresh-frozen primary ATRT (C) and sPNET (D) surgical specimens (scale bars, 50 μm). (**E**) ATRT or sPNET cells were incubated with human macrophages in the presence of Hu5F9-G4 or human IgG, and phagocytosis was observed by fluorescence microscopy. Hu5F9-G4 significantly enhanced phagocytosis of ATRT cells ($P = 0.02$) and PNET cells ($P = 0.02$). (**F**) Treatment scheme for mice bearing SU_ATRT002. (**G** and **H**) BLI images (G) and measurements (H) of SU_ATRT002 xenografts treated with either Hu5F9-G4 or control ($P < 0.0001$). (**I**) Significant survival extension was observed in mice upon Hu5F9-G4 treatment ($n = 10$ per group; $P < 0.0001$, log-rank analysis). (**J**) H&E staining of the control and Hu5F9-G4–treated SU_ATRT002 xenografts (scale bars, 2 mm). (**K**) F4/80 staining of macrophages showed increased infiltration of macrophages in tumors treated with Hu5F9-G4 compared to controls (scale bars, 50 μm). (**L**) Treatment scheme of the mice xenografted with sPNET. (**M** and **N**) BLI images (M) and measures (N) of mice bearing sPNET xenografts 28 days after treatment with either Hu5F9-G4 or control ($P = 0.0079$). (**O**) Significant increase in survival of sPNET xenografts treated with Hu5F9-G4 was seen compared to the control group (sPNET: $n = 10$ per group; $P < 0.0001$, log-rank analysis). (**P**) H&E staining of the control and Hu5F9-G4–treated mouse xenografts showed the presence of very small residual tumors in the treated group compared with the controls (scale bars, 2 mm). (**Q**) F4/80 staining of macrophages showed increased infiltration of macrophages in tumors treated with Hu5F9-G4 compared to controls (scale bars, 50 μm).

counterparts ($P < 0.0001$) (Fig. 5L). H&E staining showed reduced tumor burden (Fig. 5M), and IHC staining against the macrophage marker F4/80 indicated increased infiltration of macrophages in Hu5F9-G4–treated cohorts versus controls (Fig. 5N). GFP- and luciferase-expressing SU-DIPGXIII and JHH_DIPGI cells were injected into the pons of NSG mice, and after verification of engraftment with BLI, the mice were randomized for treatment trial (Fig. 5O and fig. S15A). Significant reduction in SU-DIPGXIII and JHH_DIPGI burden was shown by BLI measures 50 and 28 days after treatment initiated with HU5F9-G4 ($P < 0.0001$, $P = 0.0286$) (Fig. 5, P and Q, and

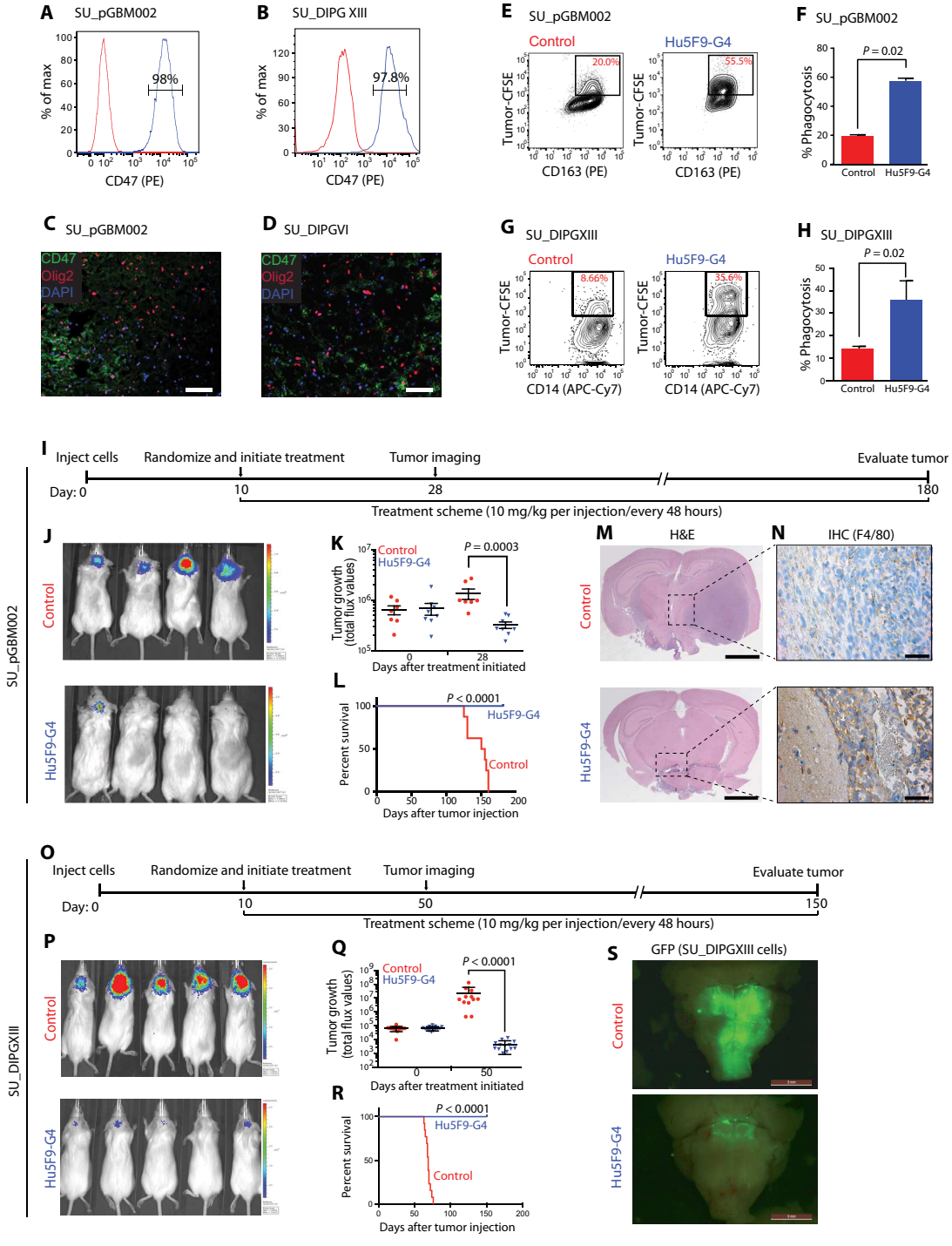

Fig. 5. Hu5F9-G4 targets pGBM and DIPG in vitro and in vivo. (**A** and **B**) Representative flow cytometric plots of surface expression of CD47 on pGBM (A) and DIPG (B). (**C** and **D**) Immunofluorescence analysis of CD47 (green) and Olig2 (red) in pGBM (C) and DIPG (D) fresh-frozen patient samples (scale bars, 50 μm). DAPI (4′,6-diamidino-2-phenylindole) nuclear stain is blue. (**E** and **F**) Phagocytosis assay of SU_pGBM002 by macrophages in the presence and absence of Hu5F9-G4 by flow cytometric (E) and histogram (F) plots. CFSE, carboxyfluorescein diacetate succinimidyl ester. (**G** and **H**) Phagocytosis assay of SU_DIPGXIII cells by macrophages in the presence or absence of Hu5F9-G4 by flow cytometric (G) and histogram (H) plots. (**I**) Treatment scheme of SU_GBM002–bearing mice. Luciferase-expressing SU_pGBM002 cells were injected into the left hemisphere of NSG mice. The treatment commenced after the tumor was detected by BLI. (**J** and **K**) BLI images (J) and measures (K) were analyzed after 28 days of treatment with either control or Hu5F9-G4. (**L**) A significant increase in survival was observed after Hu5F9-G4 administration in treated groups versus the controls [$n = 7$ (control) and $n = 8$ (Hu5F9-G4); $P < 0.0001$, log-rank analysis]. (**M**) H&E staining of SU_pGBM002 xenografted mouse revealed the spread of tumor in the control versus the treated group (scale bars, 2 mm). (**N**) F4/80 staining of xenografted mouse brains showed increased infiltration of macrophages in Hu5F9-G4–treated tumor compared to the control (scale bars, 50 μm). (**O**) Treatment scheme of SU_DIPGXIII xenografts. SU_DIPGXIII cells were injected into the pons of NSG mice. (**P** and **Q**) BLI images (P) and quantities (Q) revealed a significant decrease of tumor size in treated mice with Hu5F9-G4 compared to the control ($P < 0.0001$). (**R**) A significant increase in survival was observed after Hu5F9-G4 administration in treated groups versus control counterparts [$n = 12$ (control) and $n = 13$ (Hu5F9-G4); $P < 0.0001$, log-rank analysis]. (**S**) Efficacy of Hu5F9-G4 treatment against DIPG is represented by stereo fluorescence whole-mount microscopy in mice with GFP-expressing SU_DIPGXIII xenografted into the pons (scale bars, 5 mm).

fig. S15, B and C). Survival analysis revealed a significant survival extension in mice treated with HU5F9-G4 compared to the control group ($P < 0.0001$, $P = 0.0069$) (Fig. 5R and fig. S15D). Fluorescence stereomicroscopy of SU_DIPGXIII-GFP xenotransplanted mouse brains showed high infiltration of GFP-expressing cells in the pons of the control mice (Fig. 5S, top) compared with a minimal presence of tumor cells in the treated group (Fig. 5S, bottom). These results indicate that Hu5F9-G4 has extensive in vitro and in vivo activity against pGBM and DIPG, two of the deadliest pediatric brain tumors.

Anti-mouse CD47 mAb inhibits tumor growth and prolongs survival in an immunocompetent syngeneic model

We next tested the safety and efficacy of targeting the CD47-SIRPα axis in mice with an intact immune system. We used a well-characterized

mouse HGG cell line, GL261 (*41*). GL261 cells treated with anti-mouse CD47 (mCD47) mAb (clone MIAP410) were efficiently phagocytized by bone marrow macrophages derived from C57BL/6 mice, in contrast to GL261 cells treated with IgG alone (Fig. 6, A and B). An in vivo study was performed by orthotopically implanting GL261 cells into the brains of C57BL/6 mice. After implantation with GL261 luciferase-expressing cells, tumor engraftment was confirmed by BLI. Mice were randomized into mCD47 mAb–treated (16 mg/kg, daily) and control groups (Fig. 6C). Tumor growth assessed on days 10 and 23 of treatment demonstrated a lower rate of tumor growth in treated mice versus the control group (Fig. 6, D and E). Whereas mice in the control cohort had a median survival of 21 days, mice treated with mCD47 mAb had a prolonged median survival of 32 days (Fig. 6F). A dose-dependent response was seen when the antibody was increased to 32 mg/kg compared with 16 mg/kg of mCD47 mAb, with median survival of the mice receiving the higher dose increased to 38 days (Fig. 6F). We confirmed lower tumor burden in the mCD47 mAb–treated cohort by H&E staining (Fig. 6G) and increased accumulation of peritumoral macrophages by F4/80 staining compared with the control group (Fig. 6H). To assess the toxicity of mCD47 mAb on GL261-allografted mouse brains, we stained the brains with cresyl violet (Nissl) (Fig. 6I) and performed IHC against glial fibrillary acidic protein (GFAP) (Fig. 6J) to characterize neurons and astrocytes, respectively. Normal brain tissue surrounding the tumor revealed no damage to neurons or astrocytes and no signs of gliosis in the treated brains (Fig. 6, I and J, bottom) compared with controls (Fig. 6, I and J, top), as determined by blinded analysis with a board-certified neuropathologist. Therefore, the disruption of the CD47-SIRPα axis in a fully immunocompetent setting resulted in antitumor effects against a mouse malignant glioma allograft.

To investigate the contribution of CD47 expression to tumor growth, we knocked down CD47 in GL261 cells using a mouse CD47 shRNA (short hairpin RNA) (GL261:CD47-KD). Reduction in cell surface CD47 by shRNA was confirmed by flow cytometry (fig. S16A), and total CD47 protein content was assayed by Western blot analysis (fig. S16B). In vivo BLI revealed significantly reduced tumor growth (fig. S16, C to E) and increased survival (fig. S16F) in mice transplanted

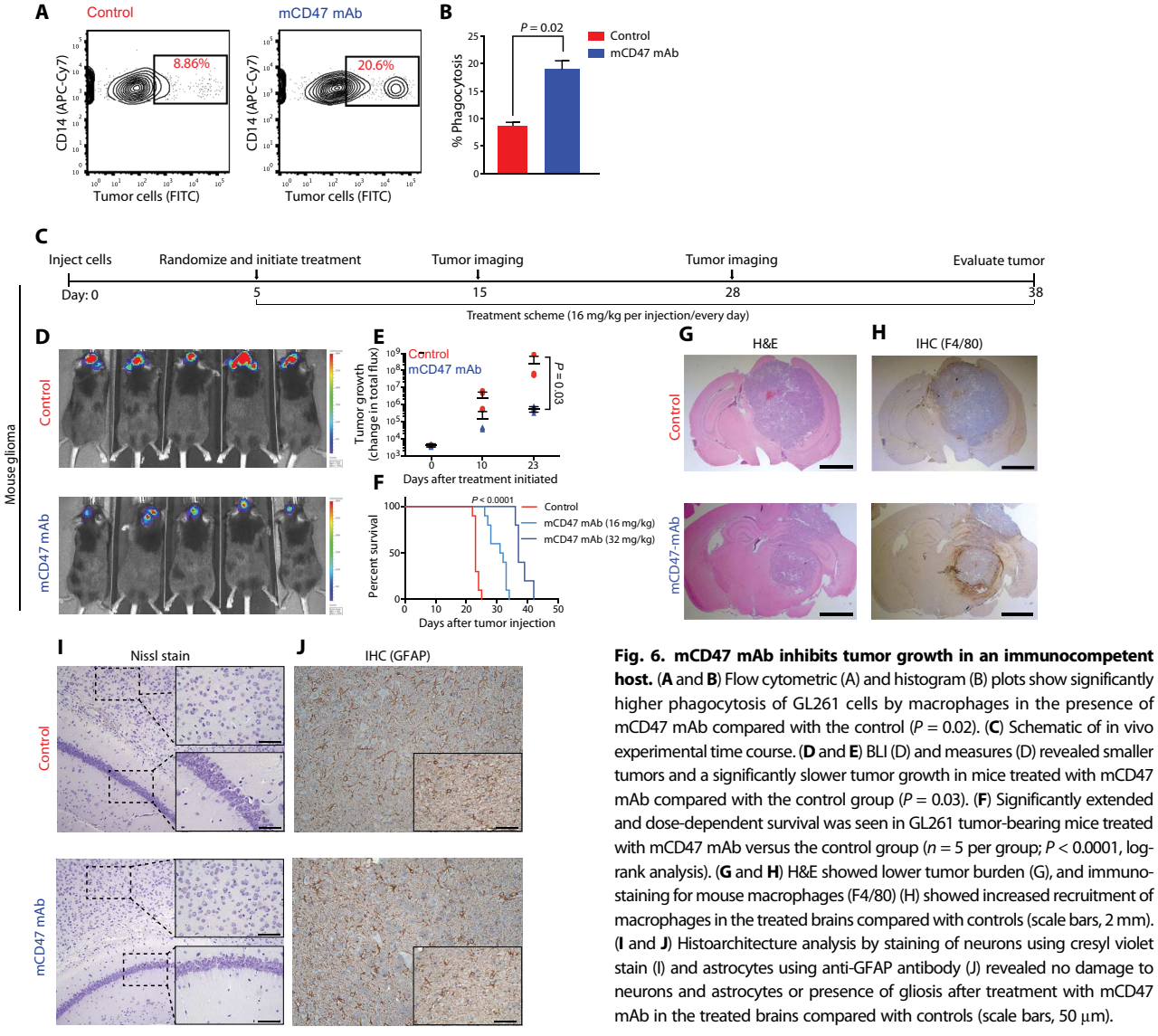

Fig. 6. mCD47 mAb inhibits tumor growth in an immunocompetent host. (**A** and **B**) Flow cytometric (A) and histogram (B) plots show significantly higher phagocytosis of GL261 cells by macrophages in the presence of mCD47 mAb compared with the control ($P = 0.02$). (**C**) Schematic of in vivo experimental time course. (**D** and **E**) BLI (D) and measures (D) revealed smaller tumors and a significantly slower tumor growth in mice treated with mCD47 mAb compared with the control group ($P = 0.03$). (**F**) Significantly extended and dose-dependent survival was seen in GL261 tumor-bearing mice treated with mCD47 mAb versus the control group ($n = 5$ per group; $P < 0.0001$, log-rank analysis). (**G** and **H**) H&E showed lower tumor burden (G), and immunostaining for mouse macrophages (F4/80) (H) showed increased recruitment of macrophages in the treated brains compared with controls (scale bars, 2 mm). (**I** and **J**) Histoarchitecture analysis by staining of neurons using cresyl violet stain (I) and astrocytes using anti-GFAP antibody (J) revealed no damage to neurons and astrocytes or presence of gliosis after treatment with mCD47 mAb in the treated brains compared with controls (scale bars, 50 μm).

with GL261:CD47-KD cells compared to control ($P = 0.0002$). Furthermore, IHC staining for F4/80 showed increased presence of macrophages in mouse brains with GL261:CD47-KD cells compared to control GL261 cells (fig. S16G).

DISCUSSION

The treatment of malignant pediatric brain tumors remains suboptimal, particularly in instances in which irradiation and intensive chemotherapy are not viable options, especially in children younger than 3 years of age. In the case of pediatric thalamic GBM and DIPG, tumor resection itself is not an option because of the surgically challenging anatomic location. Furthermore, successful clinical intervention in pediatric patients comes at a price that may include white and gray matter abnormalities, microvascular occlusions, demyelination, and calcifications, any of which can cause serious complications and permanent neurologic and cognitive deficits (*42*–*44*). Hence, there is a critical need for therapies that minimize the effects on the developing brain of a child. Because of disparate tolerability and pharmacokinetics of pharmaceutical agents between adult and pediatric patients, as well as the different biology of pediatric brain tumors, we conducted an extensive preclinical in vitro and in vivo analysis of Hu5F9-G4 against five different types of malignant pediatric brain tumors. We observed ubiquitous expression of CD47 on the cell surface in all malignant pediatric brain tumors tested by flow cytometry and by immunofluorescence staining of tissue sections. Hu5F9-G4 robustly induced phagocytosis by both human and mouse macrophages in all pediatric malignant primary brain tumors tested. Hu5F9-G4 reduced tumor burden and prolonged overall survival of group 3 MB, ATRT, PNET, pGBM, and DIPG patient-derived orthotopic xenograft models.

In the case of MB, systemic treatment with Hu5F9-G4 was effective not only against the primary site but also against leptomeningeal forebrain and spinal metastasis. Direct delivery into the CSF accelerated the antitumor effect on disseminated metastatic disease both in the forebrain and in the spine. In most of the patients with MB, primary tumor is removed by surgery. However, recurrence often occurs by metastatic leptomeningeal dissemination, which is impossible to treat surgically (*45*). The presence of metastatic disease at primary presentation or recurrence after treatment is more pronounced in the group 3 (*cMYC*-driven) subtype (*26*). Our results demonstrate potent antitumoral activity of Hu5F9-G4 against leptomeningeal disease when delivered intraperitoneally and an even greater clearance of this spread when the treatment was delivered directly into the CSF. It is possible that direct ventricular delivery of Hu5F9-G4 with or without systemic administration for treatment of patients with advanced metastatic disease may prove more efficacious in the clinical setting. Furthermore, we observed a remarkable decrease in $CD15^+$ tumor-initiating MB cells after Hu5F9-G4 treatment, suggesting Hu5F9-G4 as a viable therapeutic agent for eliminating CSCs and potentially preventing tumor relapse (*46*, *47*).

We carried out detailed evaluation of Hu5F9-G4 activity toward normal human CNS cells, including proliferating neural progenitors (which would be present in developing pediatric patients). We show a tumor-specific effect, with minimal direct or bystander toxicity toward nonneoplastic cells in vitro and in vivo, similar to our previous studies where blocking anti-CD47 antibodies reduced tumor burden in xenograft models of human leukemias and lymphomas with little to no reduction of hematopoietic stem and progenitor cells (*8*, *11*). These findings in pediatric brain tumors and hematologic malignancies are consistent with the hypothesis that malignant cells express both eat me and don't eat me signals on the cell surface. Blocking the don't eat me signal results in elimination of the tumor because of the dominance of the eat me signals. In contrast to cancer cells, normal cells have no or minimal eat me signals; therefore, blocking the don't eat me signal leaves most of these cells unaffected (*20*).

Although CD47 is highly expressed on tumor cells, there are varying degrees of expression on normal cells, raising the concern of decreased potency due to an antibody sink and potential toxicity. However, we demonstrate here that treatment of mouse glioma orthotopic allografts with mCD47 mAb in an immunocompetent model produced an effective antitumor response and prolonged survival with no sign of toxicity as shown previously (*13*).

The direct mechanism of antibody transport through the blood-brain barrier is unknown; however, our results show positive anti-IgG4 (corresponding to IgG4 Fc isotype of Hu5F9-G4) staining in the tumor tissue bed, corroborating the effective infusion of Hu5F9-G4 in treated brains. Growing evidence suggests that the CNS is immunocompetent and interacts dynamically with the systemic immune system (*48*). The blood-brain barrier itself can be compromised by malignant brain tumors (*49*), which allows for increased entry of antibodies. During inflammation, immune cells migrate into the parenchyma by chemotaxis, traveling through cytokine gradients induced by interferon-γ, a key proinflammatory myeloid activator, among others (*50*). Moreover, FcRn (neonatal Fc receptor), a ubiquitous immunoglobulin receptor highly expressed in blood vessels in the brain, can facilitate IgG transport into the CNS (*51*). All these mechanisms point toward antibody-based immunotherapies as a viable option against malignant brain tumors.

Currently, next-generation immunotherapies such as checkpoint inhibitors and other regulators of adaptive immune responses are in trials for various cancers. It is possible that tumor phagocytosis in vivo will reflect the in vitro demonstration that macrophages can cross-present class I tumor peptides to CD8 T cells, stimulating cell division and maturation to killer T cells (*52*, *53*). Thus, activation of macrophage phagocytosis with the facilitation of anti-CD47 antibodies may not only result in direct therapeutic benefit but may also restimulate antitumor T cells, which, alone or with checkpoint inhibitor antibodies, could improve the outcomes in children with malignant brain tumors.

Although CD47 blockade has shown promising potential against brain tumors, in many cases, it does not completely eliminate tumors (*11*, *13*). This could be due to pharmacokinetic limitations because penetrance of antibodies decreases with molecular weight (*54*). Furthermore, cancer specimens intrinsically differ in their susceptibility to phagocytosis (*11*, *13*, *55*), and CD47 blockade or knockout is not sufficient to induce phagocytosis but requires an additional pro-phagocytic stimulus such as opsonizing antibodies and surface exposure of CRT. An additional limitation of this study is the use of immunocompromised xenograft models, which lack B, T, and NK cells. The CD47/SIRPα axis is an early checkpoint in immune activation regulating phagocytosis and antigen uptake to subsequently promote antigen presentation to T cells by both macrophages and dendritic cells (*52*, *53*). Within a fully immunocompetent setting, the presence of immunosuppressive cells such as T regulatory cells and myeloid-derived suppressor cells could limit antitumor responses. Future experiments combining anti-CD47 with tumor-specific opsonizing antibodies, immunosuppressive cell–depleting reagents, and cytotoxic therapies such as radiation and chemotherapy, which increase CRT exposure, will be required

for harnessing the full potential of anti-CD47–mediated myeloid checkpoint therapy.

MATERIALS AND METHODS

Study design

The objective of this study was to determine the preclinical efficacy of Hu5F9-G4 as an effective treatment against malignant pediatric brain tumors. Flow cytometry and immunofluorescence staining were used to evaluate surface expression of CD47 on tumor tissues. In vitro phagocytosis assays by flow cytometry or immunofluorescence were carried out by using cell lines from different pediatric brain tumors as targets and human PBMC or mouse bone marrow–derived macrophages as effector cells. Human PBMCs from at least three different donors were used against each cell line. Tumor formation was monitored by BLI on IVIS spectrum (Caliper Life Sciences) and quantified with Living Image 4.0 software (PerkinElmer). The mice were excluded if no tumor engraftment was detected. On the basis of preliminary pilot experiments for each type of tumor xenograft, we estimated the sample size to ensure adequate statistical power. To allocate animals to experimental groups, we measured BLI from region of interest using Living Image 4.0 software and randomized the animals with www.randomizer.org. All in vivo experiments were repeated at least two times. Blinding was not performed. Mice were sacrificed to assess tumor burden and macrophage recruitment in situ. Pharmacokinetics and penetrance of Hu5F9-G4 in brain, blood, and CSF were measured. To assess the toxicity of Hu5F9-G4, we developed a sequential xenotransplant model and carried out in situ analysis of tissue after treatment with Hu5F9-G4. All in vivo experiments were repeated at least two times, unless mentioned otherwise.

Statistical analysis

All statistical analyses were performed using GraphPad Prism 6 software. Results were expressed as means ± SD. Mann-Whitney test was used for group comparisons (two-tailed). Survival analysis was performed using log-rank test. $P < 0.05$ was considered significant.

Bioinformatics analysis

Using R2 software and the megasampler function (http://r2.amc.nl), we compared CD47 mRNA expression patterns in various gene expression profiling studies including brain tumor ($n = 861$) and normal samples ($n = 225$; both deposited in http://r2.amc.nl). In a second analysis, we delineated CD47 mRNA expression in MBs ($n = 195$). Subgroup-specific gene expression profiling differences were determined in three gene expression profiling studies (*4*, *36*) including independent MB cohorts. The following data sets were analyzed for CD47 mRNA expression across various types of pediatric brain tumors and normal brain samples: Toronto [GEO (Gene Expression Omnibus) ID: GSE21140], Heidelberg (GEO ID: GSE28245), Boston (courtesy of Y.-J.C.), MAGIC (GEO ID: GSE37382), Kool (GEO ID: GSE10327), and Gilbertson (GEO ID: GSE37418). These data sets are available at http://hgserver1.amc.nl/cgi-bin/r2/main.cgi?&species=hs.

SUPPLEMENTARY MATERIALS

www.sciencetranslationalmedicine.org/cgi/content/full/9/381/eaaf2968/DC1

Materials and Methods

Fig. S1. Expression analysis of CD47 and cell surface CRT in MB.

Fig. S2. Induction of potent macrophage-mediated phagocytosis of MB cells derived from surgical specimens by Hu5F9-G4.

Fig. S3. Flow cytometry gating strategy.

Fig. S4. Verification of phagocytic activity.

Fig. S5. Representative tumor burden at treatment initiation.

Fig. S6. Efficacy and dose-dependent response of Hu5F9-G4 in cell line–derived *cMYC*-amplified MB xenografts.

Fig. S7. Pharmacokinetic analysis and brain penetrance of Hu5F9-G4.

Fig. S8. Flow cytometric analysis of myeloid cell infiltration after Hu5F9-G4 treatment.

Fig. S9. Efficacy of Hu5F9-G4 against a primary patient-derived MB xenograft.

Fig. S10. Stability of Hu5F9-G4.

Fig. S11. Evaluating the toxicity of Hu5F9-G4 against human normal neural cells.

Fig. S12. CD47 and CRT expression on primary pediatric brain tumor samples.

Fig. S13. Macrophage-mediated phagocytosis of pediatric brain tumor cells.

Fig. S14. High expression of Olig2 and Nestin on $CD47^+$ DIPG cells.

Fig. S15. Efficacy of Hu5F9-G4 in JHH-DIPGI xenografts.

Fig. S16. Contribution of CD47 expression to tumor growth and phagocytosis by macrophages in an immunocompetent setting.

Table S1. Quantitative IHC assessment of macrophage infiltration in vivo.

Table S2. General characteristics of cell lines used in the study.

Movie S1. Qualitative behavioral assessment of SU_MB002 tumor-bearing mice treated with Hu5F9-G4 compared to control.

Movie S2. Qualitative behavioral assessment of D425s tumor-bearing mice treated with Hu5F9-G4 compared to control.

Reference (*56*)

REFERENCES AND NOTES

1. I. F. Pollack, R. I. Jakacki, Childhood brain tumors: Epidemiology, current management and future directions. *Nat. Rev. Neurol.* **7**, 495–506 (2011).
2. I. F. Pollack, Multidisciplinary management of childhood brain tumors: A review of outcomes, recent advances, and challenges. *J. Neurosurg. Pediatr.* **8**, 135–148 (2011).
3. B. L. Maria, K. Rehder, T. A. Eskin, L. M. Hamed, E. B. Fennell, R. G. Quisling, J. P. Mickle, R. B. Marcus, W. E. Drane, N. P. Mendenhall, W. M. McCollough, A. Kedar, Brainstem glioma: I. Pathology, clinical features, and therapy. *J. Child Neurol.* **8**, 112–128 (1993).
4. P. A. Northcott, A. Korshunov, H. Witt, T. Hielscher, C. G. Eberhart, S. Mack, E. Bouffet, S. C. Clifford, C. E. Hawkins, P. French, J. T. Rutka, S. Pfister, M. D. Taylor, Medulloblastoma comprises four distinct molecular variants. *J. Clin. Oncol.* **29**, 1408–1414 (2011).
5. S. M. Castellino, N. J. Ullrich, M. J. Whelen, B. J. Lange, Developing interventions for cancer-related cognitive dysfunction in childhood cancer survivors. *J. Natl. Cancer Inst.* **106**, dju186 (2014).
6. C. M. Suryadevara, T. Verla, L. Sanchez-Perez, E. A. Reap, B. D. Choi, P. E. Fecci, J. H. Sampson, Immunotherapy for malignant glioma. *Surg. Neurol. Int.* **6**, S68–S77 (2015).
7. E. J. Brown, W. A. Frazier, Integrin-associated protein (CD47) and its ligands. *Trends Cell Biol.* **11**, 130–135 (2001).
8. S. Jaiswal, C. H. M. Jamieson, W. W. Pang, C. Y. Park, M. P. Chao, R. Majeti, D. Traver, N. van Rooijen, I. L. Weissman, CD47 is upregulated on circulating hematopoietic stem cells and leukemia cells to avoid phagocytosis. *Cell* **138**, 271–285 (2009).
9. D. Traver, K. Akashi, I. L. Weissman, E. Lagasse, Mice defective in two apoptosis pathways in the myeloid lineage develop acute myeloblastic leukemia. *Immunity* **9**, 47–57 (1998).
10. S. Jaiswal, D. Traver, T. Miyamoto, K. Akashi, E. Lagasse, I. L. Weissman, Expression of BCR/ABL and BCL-2 in myeloid progenitors leads to myeloid leukemias. *Proc. Natl. Acad. Sci. U.S.A.* **100**, 10002–10007 (2003).
11. R. Majeti, M. P. Chao, A. A. Alizadeh, W. W. Pang, S. Jaiswal, K. D. Gibbs Jr., N. van Rooijen, I. L. Weissman, CD47 is an adverse prognostic factor and therapeutic antibody target on human acute myeloid leukemia stem cells. *Cell* **138**, 286–299 (2009).
12. M. P. Chao, A. A. Alizadeh, C. Tang, M. Jan, R. Weissman-Tsukamoto, F. Zhao, C. Y. Park, I. L. Weissman, R. Majeti, Therapeutic antibody targeting of CD47 eliminates human acute lymphoblastic leukemia. *Cancer Res.* **71**, 1374–1384 (2011).
13. S. B. Willingham, J.-P. Volkmer, A. J. Gentles, D. Sahoo, P. Dalerba, S. S. Mitra, J. Wang, H. Contreras-Trujillo, R. Martin, J. D. Cohen, P. Lovelace, F. A. Scheeren, M. P. Chao, K. Weiskopf, C. Tang, A. K. Volkmer, T. J. Naik, T. A. Storm, A. R. Mosley, B. Edris, S. M. Schmid, C. K. Sun, M.-S. Chua, O. Murillo, P. Rajendran, A. C. Cha, R. K. Chin, D. Kim, M. Adorno, T. Raveh, D. Tseng, S. Jaiswal, P. Ø. Enger, G. K. Steinberg, G. Li, S. K. So, R. Majeti, G. R. Harsh, M. van de Rijn, N. N. H. Teng, J. B. Sunwoo, A. A. Alizadeh, M. F. Clarke, I. L. Weissman, The CD47-signal regulatory protein alpha (SIRPa) interaction is a therapeutic target for human solid tumors. *Proc. Natl. Acad. Sci. U.S.A.* **109**, 6662–6667 (2012).
14. B. Edris, K. Weiskopf, A. K. Volkmer, J.-P. Volkmer, S. B. Willingham, H. Contreras-Trujillo, J. Liu, R. Majeti, R. B. West, J. A. Fletcher, A. H. Beck, I. L. Weissman, M. van de Rijn, Antibody therapy targeting the CD47 protein is effective in a model of aggressive metastatic leiomyosarcoma. *Proc. Natl. Acad. Sci. U.S.A.* **109**, 6656–6661 (2012).

15. D. Kim, J. Wang, S. B. Willingham, R. Martin, G. Wernig, I. L. Weissman, Anti-CD47 antibodies promote phagocytosis and inhibit the growth of human myeloma cells. *Leukemia* **26**, 2538–2545 (2012).
16. A. N. Barclay, T. K. van den Berg, The interaction between signal regulatory protein alpha (SIRPα) and CD47: Structure, function, and therapeutic target. *Annu. Rev. Immunol.* **32**, 25–50 (2014).
17. S. J. Gardai, K. A. McPhillips, S. C. Frasch, W. J. Janssen, A. Starefeldt, J. E. Murphy-Ullrich, D. L. Bratton, P.-A. Oldenborg, M. Michalak, P. M. Henson, Cell-surface calreticulin initiates clearance of viable or apoptotic cells through *trans*-activation of LRP on the phagocyte. *Cell* **123**, 321–334 (2005).
18. S. J. Gardai, D. L. Bratton, C. A. Ogden, P. M. Henson, Recognition ligands on apoptotic cells: A perspective. *J. Leukoc. Biol.* **79**, 896–903 (2006).
19. M. P. Chao, I. L. Weissman, R. Majeti, The CD47-SIRPα pathway in cancer immune evasion and potential therapeutic implications. *Curr. Opin. Immunol.* **24**, 225–232 (2012).
20. M. P. Chao, S. Jaiswal, R. Weissman-Tsukamoto, A. A. Alizadeh, A. J. Gentles, J. Volkmer, K. Weiskopf, S. B. Willingham, T. Raveh, C. Y. Park, R. Majeti, I. L. Weissman, Calreticulin is the dominant pro-phagocytic signal on multiple human cancers and is counterbalanced by CD47. *Sci. Transl. Med.* **2**, 63ra94 (2010).
21. M. P. Chao, C. Tang, R. K. Pachynski, R. Chin, R. Majeti, I. L. Weissman, Extranodal dissemination of non-Hodgkin lymphoma requires CD47 and is inhibited by anti-CD47 antibody therapy. *Blood* **118**, 4890–4901 (2011).
22. J. Liu, L. Wang, F. Zhao, S. Tseng, C. Narayanan, L. Shura, S. Willingham, M. Howard, S. Prohaska, J. Volkmer, M. Chao, I. L. Weissman, R. Majeti, Pre-clinical development of a humanized anti-CD47 antibody with anti-cancer therapeutic potential. *PLOS ONE* **10**, e0137345 (2015).
23. M. Kool, A. Korshunov, M. Remke, D. T. W. Jones, M. Schlanstein, P. A. Northcott, Y.-J. Cho, J. Koster, A. Schouten-van Meeteren, D. van Vuurden, S. C. Clifford, T. Pietsch, A. O. von Bueren, S. Rutkowski, M. McCabe, V. P. Collins, M. L. Bäcklund, C. Haberler, F. Bourdeaut, O. Delattre, F. Doz, D. W. Ellison, R. J. Gilbertson, S. L. Pomeroy, M. D. Taylor, P. Lichter, S. M. Pfister, Molecular subgroups of medulloblastoma: An international meta-analysis of transcriptome, genetic aberrations, and clinical data of WNT, SHH, Group 3, and Group 4 medulloblastomas. *Acta Neuropathol.* **123**, 473–484 (2012).
24. T.-A. Read, M. P. Fogarty, S. L. Markant, R. E. McLendon, Z. Wei, D. W. Ellison, P. G. Febbo, R. J. Wechsler-Reya, Identification of CD15 as a marker for tumor-propagating cells in a mouse model of medulloblastoma. *Cancer Cell* **15**, 135–147 (2009).
25. R. J. Ward, L. Lee, K. Graham, T. Satkunendran, K. Yoshikawa, E. Ling, L. Harper, R. Austin, E. Nieuwenhuis, I. D. Clarke, C.-c. Hui, P. B. Dirks, Multipotent $CD15^+$ cancer stem cells in *Patched-1*–deficient mouse medulloblastoma. *Cancer Res.* **69**, 4682–4690 (2009).
26. P. A. Northcott, A. Korshunov, S. M. Pfister, M. D. Taylor, The clinical implications of medulloblastoma subgroups. *Nat. Rev. Neurol.* **8**, 340–351 (2012).
27. M. Monje, P. G. Fisher, Neurological complications following treatment of children with brain tumors. *J. Pediatr. Rehabil. Med.* **4**, 31–36 (2011).
28. N. Uchida, D. W. Buck, D. He, M. J. Reitsma, M. Masek, T. V. Phan, A. S. Tsukamoto, F. H. Gage, I. L. Weissman, Direct isolation of human central nervous system stem cells. *Proc. Natl. Acad. Sci. U.S.A.* **97**, 14720–14725 (2000).
29. S. Tamaki, K. Eckert, D. He, R. Sutton, M. Doshe, G. Jain, R. Tushinski, M. Reitsma, B. Harris, A. Tsukamoto, F. Gage, I. Weissman, N. Uchida, Engraftment of sorted/expanded human central nervous system stem cells from fetal brain. *J. Neurosci. Res.* **69**, 976–986 (2002).
30. K. J. Cohen, R. L. Heideman, T. Zhou, E. J. Holmes, R. S. Lavey, E. Bouffet, I. F. Pollack, Temozolomide in the treatment of children with newly diagnosed diffuse intrinsic pontine gliomas: A report from the Children's Oncology Group. *Neuro Oncol.* **13**, 410–416 (2011).
31. A. M. Donson, D. K. Birks, V. N. Barton, Q. Wei, B. K. Kleinschmidt-Demasters, M. H. Handler, A. E. Waziri, M. Wang, N. K. Foreman, Immune gene and cell enrichment is associated with a good prognosis in ependymoma. *J. Immunol.* **183**, 7428–7440 (2009).
32. L. M. Hoffman, A. M. Donson, I. Nakachi, A. M. Griesinger, D. K. Birks, V. Amani, M. S. Hemenway, A. K. Liu, M. Wang, T. C. Hankinson, M. H. Handler, N. K. Foreman, Molecular sub-group-specific immunophenotypic changes are associated with outcome in recurrent posterior fossa ependymoma. *Acta Neuropathol.* **127**, 731–745 (2014).
33. K. Wani, T. S. Armstrong, E. Vera-Bolanos, A. Raghunathan, D. Ellison, R. Gilbertson, B. Vaillant, S. Goldman, R. J. Packer, M. Fouladi, I. Pollack, T. Mikkelsen, M. Prados, A. Omuro, R. Soffietti, A. Ledoux, C. Wilson, L. Long, M. R. Gilbert, K. Aldape; Collaborative Ependymoma Research Network, A prognostic gene expression signature in infratentorial ependymoma. *Acta Neuropathol.* **123**, 727–738 (2012).
34. S. Miller, H. A. Rogers, P. Lyon, V. Rand, M. Adamowicz-Brice, S. C. Clifford, J. T. Hayden, S. Dyer, S. Pfister, A. Korshunov, M.-A. Brundler, J. Lowe, B. Coyle, R. G. Grundy, Genome-wide molecular characterization of central nervous system primitive neuroectodermal tumor and pineoblastoma. *Neuro Oncol.* **13**, 866–879 (2011).
35. J. A. Knipstein, D. K. Birks, A. M. Donson, I. Alimova, N. K. Foreman, R. Vibhakar, Histone deacetylase inhibition decreases proliferation and potentiates the effect of ionizing radiation in atypical teratoid/rhabdoid tumor cells. *Neuro Oncol.* **14**, 175–183 (2012).
36. R. B. Roth, P. Hevezi, J. Lee, D. Willhite, S. M. Lechner, A. C. Foster, A. Zlotnik, Gene expression analyses reveal molecular relationships among 20 regions of the human CNS. *Neurogenetics* **7**, 67–80 (2006).
37. Y.-J. Cho, A. Tsherniak, P. Tamayo, S. Santagata, A. Ligon, H. Greulich, R. Berhoukim, V. Amani, L. Goumnerova, C. G. Eberhart, C. C. Lau, J. M. Olson, R. J. Gilbertson, A. Gajjar, O. Delattre, M. Kool, K. Ligon, M. Meyerson, J. P. Mesirov, S. L. Pomeroy, Integrative genomic analysis of medulloblastoma identifies a molecular subgroup that drives poor clinical outcome. *J. Clin. Oncol.* **29**, 1424–1430 (2011).
38. M. Monje, S. S. Mitra, M. E. Freret, T. B. Raveh, J. Kim, M. Masek, J. L. Attema, G. Li, T. Haddix, M. S. B. Edwards, P. G. Fisher, I. L. Weissman, D. H. Rowitch, H. Vogel, A. J. Wong, P. A. Beachy, Hedgehog-responsive candidate cell of origin for diffuse intrinsic pontine glioma. *Proc. Natl. Acad. Sci. U.S.A.* **108**, 4453–4458 (2011).
39. K. L. Ligon, E. Huillard, S. Mehta, S. Kesari, H. Liu, J. A. Alberta, R. M. Bachoo, M. Kane, D. N. Louis, R. A. Depinho, D. J. Anderson, C. D. Stiles, D. H. Rowitch, Olig2-regulated lineage-restricted pathway controls replication competence in neural stem cells and malignant glioma. *Neuron* **53**, 503–517 (2007).
40. K. L. Ligon, J. A. Alberta, A. T. Kho, J. Weiss, M. R. Kwaan, C. L. Nutt, D. N. Louis, C. D. Stiles, D. H. Rowitch, The oligodendroglial lineage marker OLIG2 is universally expressed in diffuse gliomas. *J. Neuropathol. Exp. Neurol.* **63**, 499–509 (2004).
41. J. I. Ausman, W. R. Shapiro, D. P. Rall, Studies on the chemotherapy of experimental brain tumors: Development of an experimental model. *Cancer Res.* **30**, 2394–2400 (1970).
42. R. K. Mulhern, S. L. Palmer, Neurocognitive late effects in pediatric cancer. *Curr. Probl. Cancer* **27**, 177–197 (2003).
43. J. S. Tsuruda, K. E. Kortman, W. G. Bradley, D. C. Wheeler, W. Van Dalsem, T. P. Bradley, Radiation effects on cerebral white matter: MR evaluation. *AJR Am. J. Roentgenol.* **149**, 165–171 (1987).
44. T. A. Glauser, R. J. Packer, Cognitive deficits in long-term survivors of childhood brain tumors. *Childs Nerv. Syst.* **7**, 2–12 (1991).
45. V. Ramaswamy, M. Remke, E. Bouffet, C. C. Faria, S. Perreault, Y.-J. Cho, D. J. Shih, B. Luu, A. M. Dubuc, P. A. Northcott, U. Schüller, S. Gururangan, R. McLendon, D. Bigner, M. Fouladi, K. L. Ligon, S. L. Pomeroy, S. Dunn, J. Triscott, N. Jabado, A. Fontebasso, D. T. W. Jones, M. Kool, M. A. Karajannis, S. L. Gardner, D. Zagzag, S. Nunes, J. Pimentel, J. Mora, E. Lipp, A. W. Walter, M. Ryzhova, O. Zheludkova, E. Kumirova, J. Alshami, S. E. Croul, J. T. Rutka, C. Hawkins, U. Tabori, K.-E. T. Codispoti, R. J. Packer, S. M. Pfister, A. Korshunov, M. D. Taylor, Recurrence patterns across medulloblastoma subgroups: An integrated clinical and molecular analysis. *Lancet Oncol.* **14**, 1200–1207 (2013).
46. S. Shukla, S. M. Meeran, Epigenetics of cancer stem cells: Pathways and therapeutics. *Biochim. Biophys. Acta* **1840**, 3494–3502 (2014).
47. J. D. O'Flaherty, M. Barr, D. Fennell, D. Richard, J. Reynolds, J. O'Leary, K. O'Byrne, The cancer stem-cell hypothesis: Its emerging role in lung cancer biology and its relevance for future therapy. *J. Thorac. Oncol.* **7**, 1880–1890 (2012).
48. M. J. Carson, J. M. Doose, B. Melchior, C. D. Schmid, C. C. Ploix, CNS immune privilege: Hiding in plain sight. *Immunol. Rev.* **213**, 48–65 (2006).
49. D. C. Davies, Blood–brain barrier breakdown in septic encephalopathy and brain tumours. *J. Anat.* **200**, 639–646 (2002).
50. R. S. Klein, L. Izikson, T. Means, H. D. Gibson, E. Lin, R. A. Sobel, H. L. Weiner, A. D. Luster, IFN-inducible protein 10/CXC chemokine ligand 10-independent induction of experimental autoimmune encephalomyelitis. *J. Immunol.* **172**, 550–559 (2004).
51. L. A. Lampson, Monoclonal antibodies in neuro-oncology: Getting past the blood-brain barrier. *MAbs* **3**, 153–160 (2011).
52. D. Tseng, J.-P. Volkmer, S. B. Willingham, H. Contreras-Trujillo, J. W. Fathman, N. B. Fernhoff, J. Seita, M. A. Inlay, K. Weiskopf, M. Miyanishi, I. L. Weissman, Anti-CD47 antibody-mediated phagocytosis of cancer by macrophages primes an effective antitumor T-cell response. *Proc. Natl. Acad. Sci. U.S.A.* **110**, 11103–11108 (2013).
53. X. Liu, Y. Pu, K. Cron, L. Deng, J. Kline, W. A. Frazier, H. Xu, H. Peng, Y.-X. Fu, M. M. Xu, CD47 blockade triggers T cell–mediated destruction of immunogenic tumors. *Nat. Med.* **21**, 1209–1215 (2015).
54. R. A. Beckman, L. M. Weiner, H. M. Davis, Antibody constructs in cancer therapy: Protein engineering strategies to improve exposure in solid tumors. *Cancer* **109**, 170–179 (2007).
55. K. Weiskopf, A. M. Ring, C. C. M. Ho, J.-P. Volkmer, A. M. Levin, A. K. Volkmer, E. Özkan, N. B. Fernhoff, M. van de Rijn, I. L. Weissman, K. C. Garcia, Engineered SIRPα variants as immunotherapeutic adjuvants to anticancer antibodies. *Science* **341**, 88–91 (2013).
56. P. Bandopadhayay, G. Bergthold, B. Nguyen, S. Schubert, S Gholamin, Y. Tang, S. Bolin, S. E. Schumacher, R. Zeid, S. Masoud, F. Yu, N. Vue, W. J. Gibson, B. R. Paolella, S. S. Mitra, S. H. Cheshier, J. Qi, K.-W. Liu, R. Wechsler-Reya, W. A. Weiss, F. J. Swartling, M. W. Kieran, J. E. Bradner, R. Beroukhim, Y.-J. Cho, BET bromodomain inhibition of *MYC*-amplified medulloblastoma. *Clin. Cancer Res.* **20**, 912–925 (2014).

Acknowledgments: We thank J. Marcellus and M. Coburn at the Stanford University Department of Neurosurgery Brain Bank and J. Bueno and C. Cuevas at the Stanford University Tissue Bank for collection and acquisition of freshly resected tumor samples. We thank M. Lim of the Department of Neurosurgery at Johns Hopkins School of Medicine for the GL261 mouse glioma cell line. We also thank Y.-J.C. from the Oregon Health & Science University for providing us with primary patient MB and ATRT samples and D. Bigner for cell lines D283 and D425. We are grateful to the surgical support staff at the Lucile Packard Children's Hospital for their vital role in providing us with timely support for tissue acquisition. We thank the members of the Weissman and Cheshier laboratories for their help during various experiments and M. Alvarez and the staff of the Stanford University Veterinary Service Center for their help with animal husbandry. We would also like to acknowledge and thank C. J. Christensen for editing the manuscript. We especially acknowledge the patients and their parents for their consent for tissue donation for research. **Funding:** This study was supported by the Price Family Charitable Fund, the Stanford Center for Children's Brain Tumors (to S.G., S.S.M., M.M., M.E., and S.H.C.), the St. Baldrick's Foundation, the American Brain Tumor Association (to S.H.C.), the Seibel Scholars Award from the Siebel Stem Cell Institute (to S.S.M.), the Pew Latin American Fellows (to S.A.K.), the Deutsche Forschungsgemeinschaft (VO 1976/1 to A.K.V.), the National Institute of Neurological Disorders and Stroke (NINDS K08NS070926 to M.M.), the National Cancer Institute Core Grant to the Johns Hopkins Sidney Kimmel Comprehensive Cancer Center (P30 CA006973 to E.H.R.), the McKenna Claire Foundation (to M.M.), the Matthew Larson Foundation (to E.H.R. and M.M.), the California Institute for Regenerative Medicine (CIRM RB4-06093 and RN3- 06510 to M.M. and DR3-06965 to R.M. and I.L.W.), the Alex's Lemonade Stand Foundation (to M.M.), The Cure Starts Now Foundation (to M.M.), the Lyla Nsouli Foundation (to M.M.), the Dylan Jewett, Connor Johnson, Zoey Ganesh, Dylan Frick, Abigail Jensen, Wayland Villars, and Jennifer Kranz Memorial Funds (to M.M.), the Virginia and D. K. Ludwig Fund for Cancer Research (to M.M., R.M., I.L.W., and S.H.C.), the Lucile Packard Foundation for Children's Health, Child Health Research Institute at the Stanford University (NIH-NCATS-CTSA UL1 TR001085), the Tashia and John Morgridge Endowed Pediatric Faculty Scholar and Fellowships Awards (to S.H.C.), and the Anne T. and Robert M. Bass Endowed Faculty Scholarship in Pediatric Cancer and Blood Diseases (to M.M.). M.R. received a postdoctoral fellowship from the Dr. Mildred Scheel Foundation/German Cancer Aid. Y.-J.C. is supported by the Ericksen Family Endowed Professorship for Research (Oregon Health & Science University), the St. Baldrick's "Miracles for Michael" Scholar Award, and NIH U01-CA176287. E.H.R. is a St. Baldrick's Scholar. S.H.C. is the Ty Louis Campbell Foundation St. Baldrick's Scholar recipient. S.H.C. received gifts from G. Landegger, R. McDowell, V. McDowell, C. Comey, J. Huang, C. Fisher, and J. Fisher. **Author contributions:** S.G., S.S.M., I.L.W., and S.H.C. conceived the project and wrote the manuscript. J.L., S.W., J.P.V., R.M., and I.L.W. developed and characterized Hu5F9-G4. S.G., S.S.M., S.H.C., E.H.R., M.M., Y.-J.C., S.S., and A.P. generated and provided patient-derived pediatric brain tumor cells. S.G., S.S.M., C.R., and M.Z. performed phagocytosis assays. S.G., A.H.F., S.A.K., and R.E. performed in vivo experiments. G.H. supervised the brain tumor bank. S.S.M., A.M., T.A.S., A.K.V., S.W., and P.L. provided the animals, reagents, and technical support. S.H.C., G.G., G.K.S., M.E., and P.G.F. provided primary patient samples, V.R., M.R., and M.D.T. provided and analyzed gene array expression data. S.G. and P.C. carried out IHC analysis. S.G. and C.N. collected and analyzed data on blood and CSFs. H.V. contributed to tissue analysis. **Competing interests:** I.L.W. and R.M. are coinventors on multiple patents regarding CD47 antibody targeting that have been licensed to Forty Seven Inc. They serve on the board of directors and as consultants and have equity ownership. J.L. and J.P.V. are coinventors on multiple patents regarding CD47 antibody targeting that have been licensed to Forty Seven Inc. They are employees at Forty Seven Inc. and have equity ownership. **Data and materials availability:** The data sets used in this study are available at http://hgserver1.amc.nl/cgi-bin/r2/main.cgi?&species=hs.

Submitted 31 October 2014
Resubmitted 25 January 2016
Accepted 7 December 2016
Published 15 March 2017
10.1126/scitranslmed.aaf2968

Citation: S. Gholamin, S. S. Mitra, A. H. Feroze, J. Liu, S. A. Kahn, M. Zhang, R. Esparza, C. Richard, V. Ramaswamy, M. Remke, A. K. Volkmer, S. Willingham, A. Ponnuswami, A. McCarty, P. Lovelace, T. A. Storm, S. Schubert, G. Hutter, C. Narayanan, P. Chu, E. H. Raabe, G. Harsh, M. D. Taylor, M. Monje, Y.-J. Cho, R. Majeti, J. P. Volkmer, P. G. Fisher, G. Grant, G. K. Steinberg, H. Vogel, M. Edwards, I. L. Weissman, S. H. Cheshier, Disrupting the CD47-SIRPα anti-phagocytic axis by a humanized anti-CD47 antibody is an efficacious treatment for malignant pediatric brain tumors. *Sci. Transl. Med.* **9**, eaaf2968 (2017).

Science Translational Medicine

Disrupting the CD47-SIRPα anti-phagocytic axis by a humanized anti-CD47 antibody is an efficacious treatment for malignant pediatric brain tumors

Sharareh Gholamin, Siddhartha S. Mitra, Abdullah H. Feroze, Jie Liu, Suzana A. Kahn, Michael Zhang, Rogelio Esparza, Chase Richard, Vijay Ramaswamy, Marc Remke, Anne K. Volkmer, Stephen Willingham, Anitha Ponnuswami, Aaron McCarty, Patricia Lovelace, Theresa A. Storm, Simone Schubert, Gregor Hutter, Cyndhavi Narayanan, Pauline Chu, Eric H. Raabe, Griffith Harsh IV, Michael D. Taylor, Michelle Monje, Yoon-Jae Cho, Ravi Majeti, Jens P. Volkmer, Paul G. Fisher, Gerald Grant, Gary K. Steinberg, Hannes Vogel, Michael Edwards, Irving L. Weissman and Samuel H. Cheshier

Sci Transl Med **9**, eaaf2968.
DOI: 10.1126/scitranslmed.aaf2968

Brain tumors, meet macrophages

A protein called CD47 is often expressed on the surface of tumor cells, where it serves as a "don't eat me" signal that blocks macrophages from attacking the tumor. To overcome this signal and allow the macrophages to "eat" tumor cells, Gholamin *et al*. engineered a humanized antibody that blocks CD47 signaling. The researchers tested the efficacy of this antibody in patient-derived xenograft models of a variety of pediatric brain tumors. The treatment was successful at inhibiting CD47, killing tumor cells, and prolonging the animals' survival, all without toxic effects on normal tissues.

Science Translational Medicine (ISSN 1946-6242) is published by the American Association for the Advancement of Science, 1200 New York Avenue NW, Washington, DC 20005.